Article

Phase Relations in a NaFeO$_2$-SnO$_2$ (0–50 mol.% SnO$_2$) System and the Crystal Structure and Conductivity of Na$_{0.8}$Fe$_{0.8}$Sn$_{0.2}$O$_2$

Georgiy S. Shekhtman *, Elena A. Sherstobitova, Mariya S. Shchelkanova and Evgenia A. Ilyina

Institute of High Temperature Electrochemistry, Ural Branch, Russian Academy of Sciences,
20 Akademicheskaya St., 620990 Ekaterinburg, Russia; ela.sherstobitova@gmail.com (E.A.S.);
shchelkanova.mariya@mail.ru (M.S.S.); ilyina@ihte.uran.ru (E.A.I.)
* Correspondence: shekhtman@ihte.uran.ru

Abstract: With the view of developing new materials for sodium and sodium-ion power sources, NaFeO$_2$-SnO$_2$ (0–50 mol.% SnO$_2$) powders were synthesized using a solid state method, and their phase composition and crystal structure were studied. A phase of the Na$_{0.8}$Fe$_{0.8}$Sn$_{0.2}$O$_2$ composition with a layered rhombohedral structure of the α-NaFeO$_2$ type was found when the tin dioxide content was 20 mol.%. The phase produced was of an O3 structural type. O3-type phases have sufficiently good performance when used as cathode materials in sodium-ion batteries and, moreover, often have a rather high sodium-cation conductivity. A two-dimensional migration map was built using Voronoi–Dirichlet partition and TOPOS software package. The sodium-ion conductivity of Na$_{0.8}$Fe$_{0.8}$Sn$_{0.2}$O$_2$ at room temperature was rated low (10^{-8} S × cm^{-1} at 20 °C), which may be the result of channels too narrow for Na$^+$ migration. The results obtained show that the application of the compound studied in this work as a solid electrolyte in sodium power sources is unlikely. It is the potential use of Na$_{0.8}$Fe$_{0.8}$Sn$_{0.2}$O$_2$ as the active material of cathodes in Na and Na-ion power sources that presents practical interest.

Keywords: NaFeO$_2$-SnO$_2$ system; layered O3-type structure; Na$^+$-ion conductivity; two-dimensional migration map; the TOPOS program package

1. Introduction

Sodium power sources in which Na-β-Al$_2$O$_3$ and NASICON were used as solid electrolytes were considered the most promising electrochemical energy storage solution in the 1980s and 1990s [1]. Sodium–sulfur batteries were successfully developed for electric vehicles [2], spacecraft [3], and other applications [4,5]. However, they were later replaced by power sources with lithium-containing anodes, since, in spite of a considerably higher price of lithium, its use substantially increases the energy efficiency of the power source [6,7]. The appearance of a great number of high-conductivity lithium-cation solid electrolytes has made a great contribution to the successful development of lithium and lithium-ion batteries [8–11].

However, lithium is a rare metal, its abundance in the Earth's crust is low, and the possibilities of extending the use of lithium-ion batteries to larger devices, for example, electric vehicles, will be restricted by low lithium availability. Lithium production will inevitably move to poorer deposits in the near future, which will make lithium more expensive and later scarce. At the same time, reserves of cheap sodium are practically inexhaustible (e.g., the World Ocean) [12–14]. For this reason, recently, there has been a renewal of interest in sodium power sources and, consequently, an appearance of works dedicated to the investigation of new solid electrolytes with sodium-cation conductivity and new electrode materials [15–19].

Layered oxides based on Na$_x$MO$_2$ compounds [20,21], where M stands for a transition element (i.e., Ti, V, Cr, Mn, Fe, Co, and Ni) or a combination of two [22,23] or more [24] transition elements, are nowadays considered to be promising cathode materials for sodium-ion

batteries. The structural properties of such compounds are described in detail in [25,26]. It is shown that in the crystal structure of such compounds, edge-sharing MO_6 octahedra form $(MO_2)_n$ sheets between which sodium cations are inserted. Depending on the arrangement of the octahedral layers, the coordination of alkaline cations can be octahedral (O), prismatic (P), or tetrahedral (T). The number of layers within the unit cell can be different. For example, according to the denomination suggested in [25,26], structural type O3 means that alkaline cations are in octahedral coordination and the unit cell contains three layers in which they lie. O3-type phases have sufficiently good performance when used as cathode materials in sodium-ion batteries. Thus, for example, a battery with $Na_{0.8}Ni_{0.6}Sb_{0.4}O_2$ as its cathode active material delivers the capacity of 107.3 mAh/g in the voltage range of 2–4.5 V and exhibits a good capacity retention of 98.5 mAh/g after 100 cycles [22]. The $Na(Mn_{0.25}Fe_{0.25}Co_{0.25}Ni_{0.25})O_2$ cathode compound delivers an initial discharge capacity of 180 mAh/g and a specific energy density of 578 W/kg [24]. Many O3-type phases also have a rather high sodium-cation conductivity [23], which is important for cathode materials.

The layered low-temperature α-modification of $NaFeO_2$ also belongs to the O3 structural type [26]. This circumstance, and also the low cost and availability of the starting materials, prompted research into the electrochemical properties of the α-modification of $NaFeO_2$ when used as the active material of cathodes in sodium-ion power sources [27–29]. The initial results confirmed the promising outlook of α-$NaFeO_2$-based cathodes: the power source with the α-$NaFeO_2$-based cathode and sodium anode delivered a stable reversible capacity of 80–85 mAh/g at voltages below 3.4 V and good thermal stability [28]. However, at voltages above 3.5 V, α-$NaFeO_2$ undergoes irreversible structural changes related to the migration of iron ions [27], as a result of which the capacity for sodium ions intercalation and, consequently, the reversibility of the battery deteriorates considerably. It has been shown that a partial substitution of iron ions for cations of other transition metals, such as Mn, Co, Ni [30], and Ti [29,31], improves the stability of α-$NaFeO_2$-structured phases at elevated voltages. In addition, α-$NaFeO_2$-structured solid solutions in a $NaFeO_2$-TiO_2 system have been reported to exhibit a rather high sodium-cation conductivity [32]. The present paper continues research into the electrical properties and crystal structure of the phases formed in $NaFeO_2$—$M^{IV}O_2$ systems and deals with the study of phase ratios, structure, and conductivity in the $NaFeO_2$-SnO_2 system.

2. Materials and Methods

2.1. Sample Preparation

Fe_2O_3, α-modification, (analytical grade), SnO_2 (analytical grade), and Na_2CO_3 (reagent grade), all REACHIM RF, were used as starting components for synthesizing the materials under investigation. Calculated amounts of the previously dried starting reagents were weighed (FX40-CJ analytical balance, Tokyo, Japan, BMI Surplus), within the accuracy of ± 0.0001 g, and mixed by grinding with ethanol in a porcelain mortar. The obtained mixtures were then sintered in Al_2O_3 crucibles at 700 °C to decompose Na_2CO_3. Afterwards, the reaction mixtures were ground, pressed into pellets, and heated again. In the case of $NaFeO_2$, the maximum temperature of synthesis was 700 °C, and the time was 24 h. In compositions containing SnO_2, phase formation was accomplished at higher temperatures; therefore, they were synthesized at 1100–1150 °C for 16–20 h and homogenized after 8–10 h in the process. Sintered substances were crushed into the powder (particle size less than 0.05 mm) and pressed into disks, ~1 cm in diameter and 0.1–0.2 cm thick, to be further used in electrical resistance measurements. The pressed disks were sintered at 1100 °C for 4–6 h in the powder of the same composition to eliminate the possibility of the loss of sodium oxides owing to volatility at high temperatures. The open porosity of the resulting samples did not exceed 8%.

2.2. Characterization and Electrical Measurements

Phase and structural characterization of the samples during various stages of synthesis was carried out using the X-ray powder method with a Rigaku D/MAX-2200 VL/PC

X-ray diffractometer (RIGAKU, Tokyo, Japan, monochromatic Cu *Kα*-radiation generated at 40 kW, 30 mA (λ = 1.54178 Å), 2θ = 10–80° stepwise with a 0.3 s counting time and a step of 0.02°). Jade 6.5 software (Materials Data Inc., Livermore, CA, USA) was used to calculate unit cell parameters. The errors in the cell parameter calculations did not exceed 0.02%. The structural parameters were refined by the Rietveld technique using the Full Prof program [33].

To determine the migration map of Na^+ cations, we used the Voronoi–Dirichlet approach [34] implemented into the program package TOPOS [35].

The morphology and microstructure of the samples were examined by scanning electron microscopy (electron microscope TESCAN MIRA 3 LMU, Brno, Czech Republic).

Thermal analysis was carried out using a DSC 204 F1 Phoenix unit (NETZSCH, Selb, Germany). The measurement was conducted over the temperature range 25–1050 °C in air in Pt crucibles with a rate of heating of 10 °C/min. The results obtained were processed by means of NETZSCH Proteus software (STA 449 F1A 0030-M, Selb, Germany).

The electrical resistance of the samples was measured with Ag electrodes by analysis of the impedance spectrum obtained using Elins P-40x potentiostat-galvanostat (Elins, Zelenograd, Russia) with the FRA-24M module for electrochemical impedance measurements over the frequency range of 3 Hz–500 kHz. The electronic component was estimated by the DC method with gold electrodes at 20–40 mV.

3. Results and Discussion

3.1. XRD Analysis and Phase Relations

Sodium ferrite ($NaFeO_2$) exists in three crystal modifications: α, β, and γ [36]. The low-temperature α-modification of $NaFeO_2$ undergoes an irreversible transition into the β-form at 760 °C [37], and the latter turns into the γ-form when heated to ~1000 °C [38,39]. It is known that the structure of $NaFeO_2$ synthesized at temperatures below 760 °C, to a large extent, depends on the nature and structure of the starting components, especially iron oxide [36]. For instance, heating a mixture of NaOH and α-Fe_2O_3 at 200 °C yields α-$NaFeO_2$, while α-Fe_2O_3 and Na_2CO_3 used as starting components result in β-$NaFeO_2$, even if the synthesis is below 760 °C [37]. The α-form of sodium ferrite is obtained through sintering the mixture of Fe_3O_4 and Na_2CO_3 [29], and also Fe_3O_4 and Na_2O_2 [27] at 650 °C. In [31], sodium oxalate and Fe_2O_3 were used to produce α-$NaFeO_2$, and the modification of the second starting component is not specified. In this work, we used Na_2CO_3 and α-Fe_2O_3 to synthesize $NaFeO_2$. According to XRD, sintering at 700 °C yields β-modification of $NaFeO_2$, PDF2-76-0243 (Figure 1a), which is in line with the data in [36].

According to [37], β-$NaFeO_2$ should be metastable below 760 °C; however, treatment at 700 °C for 600 h did not bring about a change in the structure [36].

When tin dioxide was added to $NaFeO_2$, even in relatively small amounts (~5 mol.%), extra reflections of a rhombohedral phase with a structure close to α-$NaFeO_2$ appeared on the XRD patterns together with β-$NaFeO_2$ reflections (Figure 1b). These reflections of the rhombohedral phase grew in intensity as the tin content increased, and when it reached 20 mol.%, the lines of β-$NaFeO_2$ disappeared, and the XRD pattern for the $Na_{0.8}Fe_{0.8}Sn_{0.2}O_2$ sample contained only the reflections of the rhombohedral phase (Figure 1c). With a further increase in the content of SnO_2 reflections of $NaFeSnO_4$, PDF2-73-0425 existed on the X-ray patterns of the samples (Figure 1d,e). Thus, unlike a similar titanium-containing system [31], $NaFeO_2$-SnO_2 system was not characterized by a wide region of solid solutions with an O3-type structure.
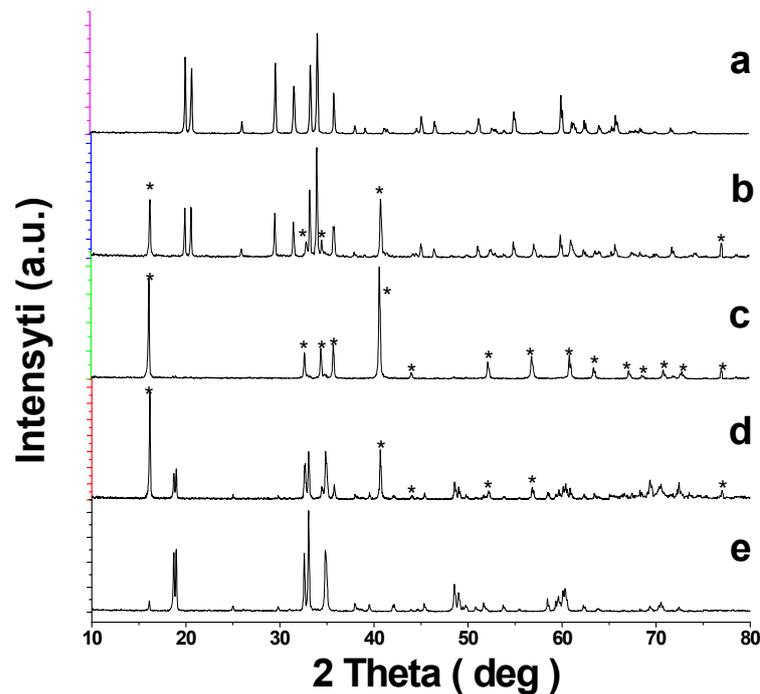
Figure 1. Powder XRD patterns for the samples of the $NaFeO_2$—SnO_2 system: (**a**) $NaFeO_2$; (**b**) 5; (**c**) 20; (**d**) 35 mol.% SnO_2; (**e**) $NaFeSnO_4$. * Designates the lines for the phases with a rhombohedral structure.

3.2. Morphology Study and Thermal Analysis

Figure 2 contains SEM images of the surface for the number of sintered pellets in the $NaFeO_2$-SnO_2 system. One can see that the microstructure of the sample that contained 5 mol.% SnO_2 (Figure 2a) was not homogeneous; it had the form of grains 1–10 μm in size and inclusions of the second phase ($NaFeO_2$-SnO_2) can be seen. The structure of the sample containing 20 mol.% SnO_2 (Figure 2b) was more homogeneous and consisted of grains 1–2 μm in size. The sample had a rather high density, though some pores can be seen. The sample containing 35 mol.% SnO_2 had a fine crystalline structure.

Figure 3 shows the DSC curves for the samples with 5, 10, and 20 mol.% SnO_2. As one can see, there were peaks at approximately1000 °C on the first two curves, while the third curve, which corresponds to the $Na_{0.8}Fe_{0.8}Sn_{0.2}O_2$ sample, contained no thermal effects. The temperature of the peaks on curves 1 and 2 was close to the ones in [38,39], which were ascribed to the β → γ transition in $NaFeO_2$. Figure 1 indicates that the content of β-phase in the samples decreased with an increase in the content of SnO_2. Returning to Figure 3, it is plain to see that the intensity of the thermal effect on the DSC curves also decreased with an increase in the tin content (Figure 3, curves 1 and 2). The sample with 20 mol.% SnO_2 contained no β-phase, and there were no peaks on the DSC curve of this sample (Figure 3, curve 3). Thus, there is every reason to believe that the thermal effects on the DSC curves (Figure 3) corresponded to the β → γ transition, while the α-solid solutions were stable across the whole temperature range studied.

The higher stability of α-solid solutions in the $NaFeO_2$-SnO_2 system, generated by the introduction and growing increase in the tin oxide content, may be explained as follows: the α-modification of $NaFeO_2$ has a rhombohedral rock-salt structure, where the Fe^{3+} ions occupy octahedral positions in the cubic closest packed oxygen layers [36], while the orthorhombic $Pbn2_1$ structure of β-$NaFeO_2$ is derived from the wurtzite structure, in which Fe cations occupy tetrahedral positions [38]. According to [40], Ti^{4+} ions often prefer octahedral coordination to the tetrahedral one. This fact is considered by the authors of [31] to be the reason for the increased stability of the α-form of $NaFeO_2$ when the ions of iron are substituted for titanium ions, which is manifested in the growing temperature of the α → β transition. The same reason may be true in the situation when iron is replaced by tin, especially since the radius of Sn^{4+} ion is bigger than the radius of Fe^{3+} (0.69 and 0.63 Å,

respectively, for the tetrahedral coordination [41]); therefore, even small amounts of added tin induce a partial transition of β-NaFeO$_2$ into α-modification, while the α → β transition does not take place with increasing temperature.

(a)

(b)

(c)
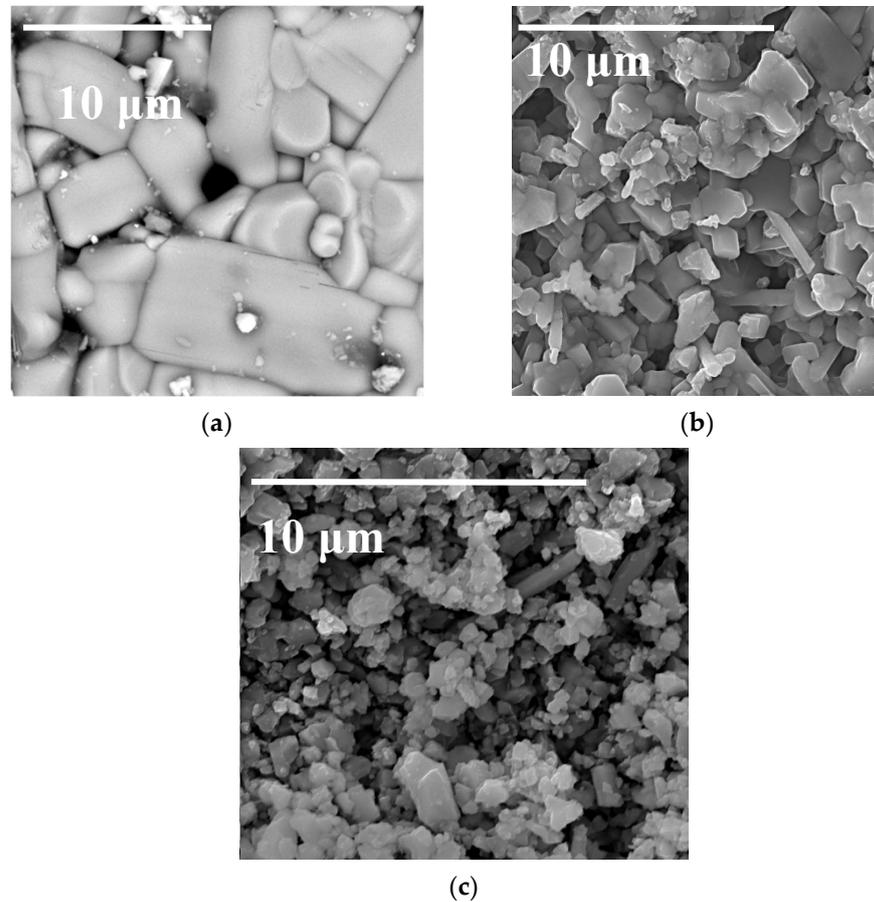
Figure 2. SEM image of the surface of the sintered Na$_{0.8}$Fe$_{0.8}$Sn$_{0.2}$O$_2$ pellets in the NaFeO$_2$-SnO$_2$ system: (**a**) 5; (**b**) 20 (Na$_{0.8}$Fe$_{0.8}$Sn$_{0.2}$O$_2$); (**c**) 35 mol.% SnO$_2$.
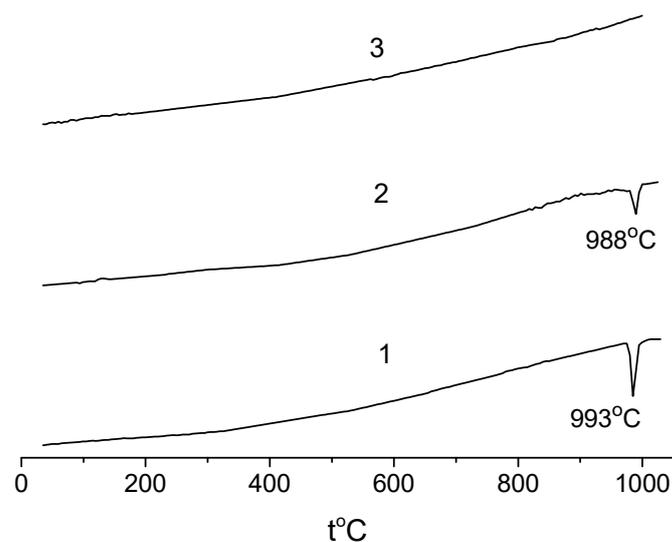
**Figure 3.** DSC curves for samples of the NaFeO$_2$—SnO$_2$ system: (1) 5; (2) 10; (3) 20 mol.% SnO$_2$.

3.3. Crystal Structure of Na$_{0.8}$Fe$_{0.8}$Sn$_{0.2}$O$_2$

Figure 4 shows Rietveld refinement using the X-ray pattern of Na$_{0.8}$Fe$_{0.8}$Sn$_{0.2}$O$_2$.
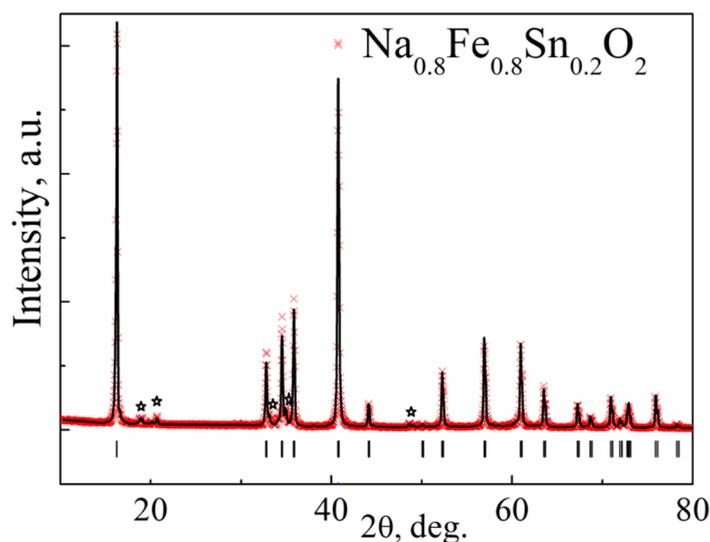
Figure 4. The result of the Rietveld refinement of the X-ray diffraction pattern of $Na_{0.8}Fe_{0.8}Sn_{0.2}O_2$. The experimental profile is represented by the red symbols ($\times$), while the calculated profile is represented by the black line. Vertical bars denote Bragg peak positions of the main rhombohedral phase (PDF2-20-1115). Asterisks mark (☆) the monoclinic impurity phase, as it was reported in Reference [37].

The diffraction pattern contained highly intensive reflections from the main phase with a rhombohedral unit cell and s. g. R-3m (No.166, PDF2-20-1115). The crystal structure of $Na_{0.8}Fe_{0.8}Sn_{0.2}O_2$ can be represented as layers of $(Fe,Sn)O_6$ octahedra alternating with layers of NaO_6 octahedra. The atoms of Na occupy 3b sites in their layer; the atoms of O occupy 6c sites. The atoms of Sn and Fe were statistically mixed in 3a sites. The crystal structure of $Na_{0.8}Fe_{0.8}Sn_{0.2}O_2$ is given in Figure 5. The refined structural parameters for the rhombohedral O3-type phase are shown in Table 1.
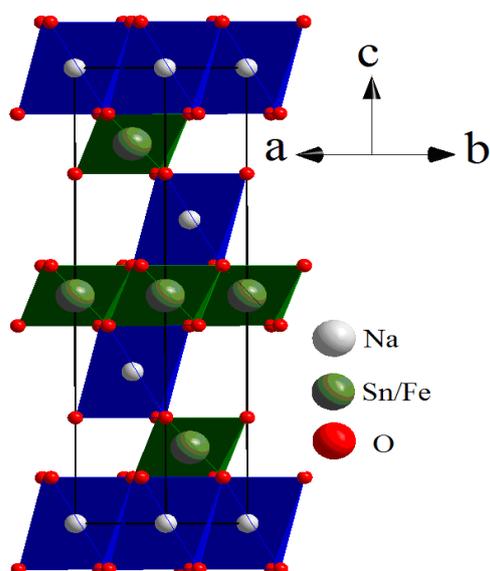
Figure 5. Rhombohedral crystal structure of $Na_{0.8}Fe_{0.8}Sn_{0.2}O_2$. Red, white, and green spheres represent oxygen, sodium, and Fe/Sn atoms, respectively.

The X-ray diffraction pattern of the $Na_{0.8}Fe_{0.8}Sn_{0.2}O_2$ sample contained additional broad reflections of low intensity at $2\theta \sim 20°$ (Figure 4), which were not connected with the main phase of the α-$NaFeO_2$ type and were apparently determined by the honeycomb-like ordering of the Fe and Sn ions within the layer. Broadening of the reflections can be

caused either by a nonideal ordering of Fe and Sn ions (the presence of a short-range order) or by a stacking fault [42]. The phase with Fe and Sn ion ordering can be satisfactorily described as a monoclinic unit cell, s.g. C2/m, and the structural model suggested for $Na_{0.89}Zn_{1/3}Ir_{2/3}O_2$ [43].

Table 1. Refined structural parameters for $Na_{0.8}Fe_{0.8}Sn_{0.2}O_2$, rhombohedral cell, s. g. R-3 m (No. 166), a = 3.0381(6), Å,c = 16.3895(4) Å.

Refined Structural Parameters	Atom		
	Na (3b)	Fe/Sn (3a)	O (6c)
Atom coordinates	001/2	000	00z
Thermal parameters, Å^2	1.31(4)	0.71(2)	0.52(4)
χ^2		3.651	
Bragg R-factor		2.91	

3.4. Conductivity Study

Undoped β-NaFeO$_2$ had a mixed electronic-ionic conductivity, where at 600–700 °C the electronic and ionic components had close values, and at lower temperatures ionic conductivity prevailed (Figure 6).
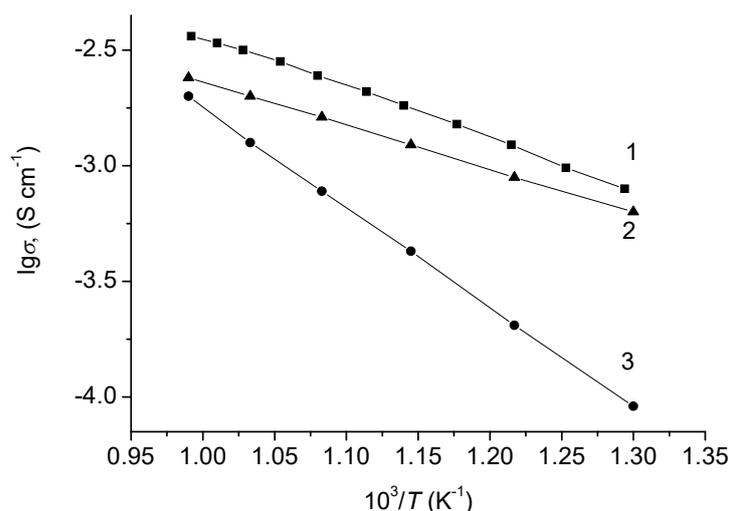
Figure 6. Temperature dependences of NaFeO$_2$ conductivity: (1) total; (2) ionic; (3) electronic conductivity.

The sodium-cation character of the ionic component of sodium ferrite conductivity was confirmed in [23]. According to the obtained results, the conductivity of NaFeSnO$_4$ was 10^{-4}–10^{-3} S × cm^{-1} over the 500–700 °C interval and was mostly ionic in character.

The conductivity of the $Na_{0.8}Fe_{0.8}Sn_{0.2}O_2$ sample was found by analysis of the impedance spectrum over the temperature range 20–370 °C. The typical impedance spectra are shown in Figure 7. In the low-temperature region, the spectra had the form of a low-frequency tail and a semicircular arc with a shifted center (Figure 7a). The total resistance, R$_{b+gb}$, of the samples under investigation was found as the values corresponding to the points of intersection between the semicircle and the Z′-axis. Above 250 °C, the spectra contained only a low-frequency tail (Figure 7b); in this case, the resistance of the sample was found by extrapolation of the low-frequency linear portion onto the real axis.
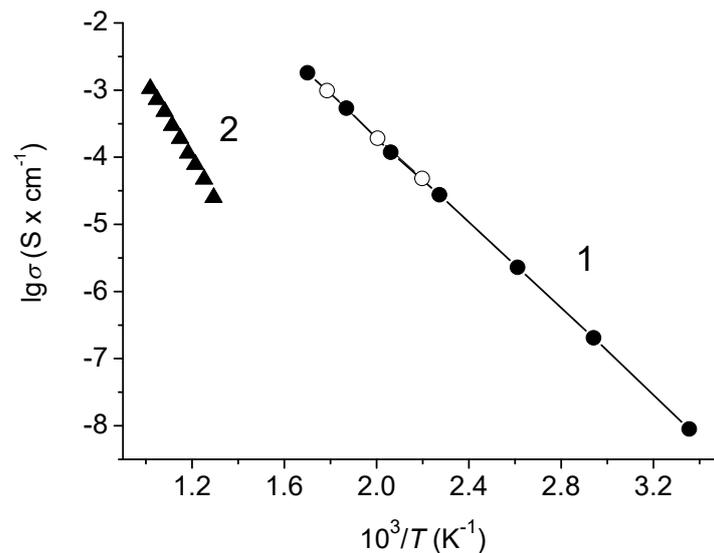
The temperature dependences of total and electronic conductivities for $Na_{0.8}Fe_{0.8}Sn_{0.2}O_2$ are given in Figure 8.

One can see that the dependence of the total conductivity in the lgσ—1/T coordinates was linear across the studied temperature range (Figure 8, line 1). The activation energy for conduction was 64.2 ± 0.43 kJ × mol^{-1}. The electronic conductivity at 500 °C was

approximately 10^{-5} S $\times$ cm^{-1} and decreased fast with the decreasing temperature (Figure 8, line 2). Thus, in the low-temperature region, $Na_{0.8}Fe_{0.8}Sn_{0.2}O_2$ was a practically unipolar sodium-cation conductor.
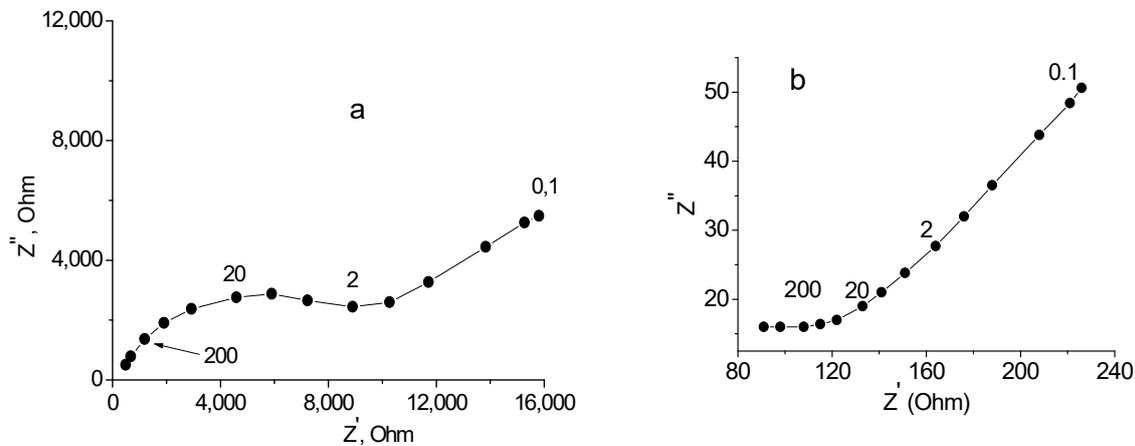
**Figure 7.** Impedance spectra for Ag | $Na_{0.8}Fe_{0.8}Sn_{0.2}O_2$ | Ag cell: (**a**) 182; (**b**) 368 °C. Numbers above the curves represent frequencies (kHz).

Figure 8. Temperature dependences of electroconductivity for $Na_{0.8}Fe_{0.8}Sn_{0.2}O_2$: (1) total conductivity; solid circles—heating, open circles—cooling; (2) electronic conductivity.

3.5. Exploration of the Migration Map of Na⁺ Cations

In order to explore the Na⁺ cations migration map (i.e., network of cations migration pathways within the crystal structure framework of the rhombohedral structure of $Na_{0.8}Fe_{0.8}Sn_{0.2}O_2$), we used the Voronoi–Dirichlet approach [35] implemented into the program package TOPOS [44]. The elementary voids and channels were searched using the Voronoi–Dirichlet polyhedra partitioning space as it was described in detail in [35]. According to this approach, vertices of the Voronoi–Dirichletpolyhedral represent centers of the elementary voids, while the edges of the Voronoi–Dirichletpolyhedral represent the elementary channel lines connecting the centers of nearby voids. In order to build the ion migration map, all elementary channels are supposed to be sorted out by using significance criteria [34]. Only "significant" voids and channels were involved in the construction of the ion migration map. According to [16], a void was considered to be significant for Na⁺ cations in an oxygen environment when the characteristic size of the void was Rsd $\geq$ (1.523 $\pm$ 0.040) Å. An elementary channel was considered to be significant when the characteristic size of the channel was Rsd $\geq$ 2.083 Å. The coordinates of the

first void, ZA1, coincided with the position of the Na atoms in the NaO_6 octahedron. The coordinates of the second void, ZA2, almost fully coincided with the coordinates of the center of the vacant tetrahedral interstitial site (2/3 1/3 0.6969) in the NaO layer. The centers of the ZA1 and ZA2 voids were connected by an elementary channel of conductivity with the radius $r = 2.048$ Å. Using the discovered ZA1 and ZA2 voids and one elementary channel of conductivity, one can build a 2D migration map in which migration channels connect the centers of NaO_6 octahedra with the vacant tetrahedron through the shared edge (see Figure 9).
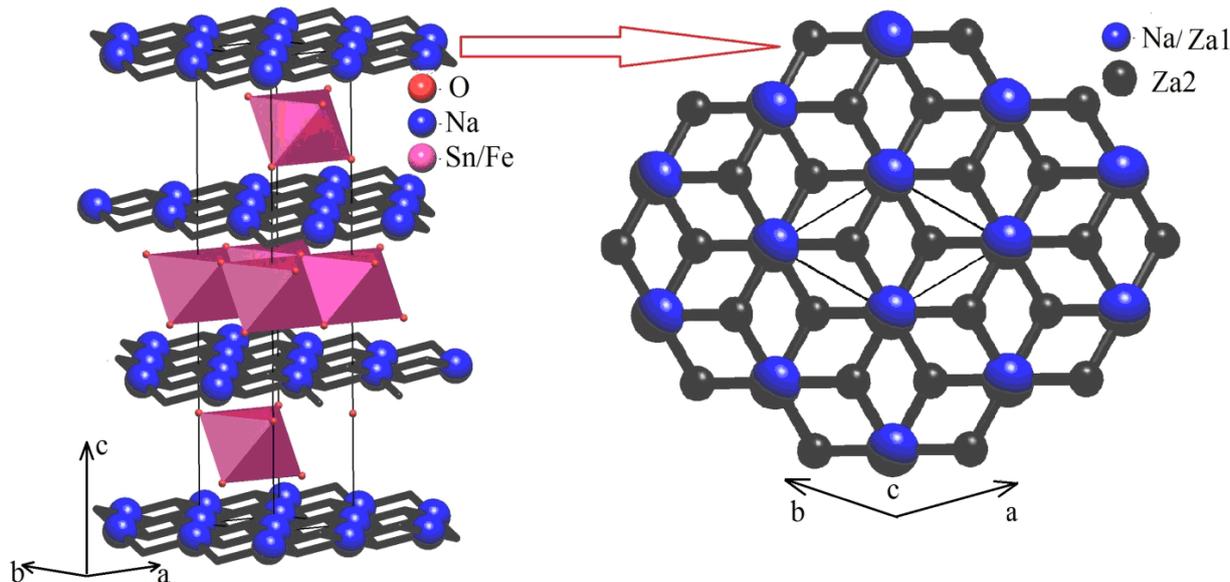
Figure 9. Migration map (**left**) and 2D migration layer (**right**) for rhombohedral $Na_{0.8}Fe_{0.8}Sn_{0.2}O_2$; large blue spheres—$Na^+$ ions coincide with Za1 significant voids, black spheres—Za2 significant voids in the center of the vacant tetrahedral interstitial site, and black lines—elementary migration channels, $Sn/FeO6$ octahedra are pink.

One can easily notice that the radius of the elementary migration channel in the lattice of the investigated compound (2.048 Å) was rather smaller compared to the critical channel diameter for Na^+ cations in oxide compounds (2.083 Å). Nevertheless, this is not the reason to exclude such channels from the migration map. Geometrical analysis and, in particular, Voronoi–Dirichlet partition, characterized the static model of a crystal structure. Migration of the charge carriers caused the crystal lattice to undergo considerable distortions and, as a result, mobile ion transfer becomes possible through the channels that are smaller than the critical size when the structure is static [45]. Insufficient width of migration channels, nevertheless, may be one of the reasons why sodium-cation conductivity of $Na_{0.8}Fe_{0.8}Sn_{0.2}O_2$ at low temperatures is rather unremarkable (10^{-8} S × cm^{-1} at 20 °C, Figure 8, line 1).

Previously the studies of $NaFeO_2$-TiO_2 system reported high sodium-cation conductivity of the obtained solid solutions, which gave reason to consider their potential application as solid electrolytes in sodium power sources [32]. The conductivity values for the $Na_{0.8}Fe_{0.8}Sn_{0.2}O_2$ phase obtained in the present work were considerably lower compared with the ones in [32]. It should also be remarked that in reducing environments, Fe^{3+} can be easily reduced to Fe^{2+}. For instance, the Na_4FeO_3 compound may form in contact with metallic sodium [46]. Sn^{4+} ions can also be reduced to Sn^{2+}. Both of these factors will lead to a sharp increase in electronic conductivity; therefore, it is highly unlikely that the compound studied in this work will be used as a solid electrolyte. $Na_{0.8}Fe_{0.8}Sn_{0.2}O_2$ is of much practical interest as the potential cathode material in Na^+ power sources. Additional electrochemical studies are required to confirm this possibility.

4. Conclusions

Samples of the NaFeO$_2$-SnO$_2$ (0–50 mol.% SnO$_2$) system were obtained by solid state synthesis for the first time, and their phase composition was studied. A novel phase having a Na$_{0.8}$Fe$_{0.8}$Sn$_{0.2}$O$_2$ composition and an O3-type rhombohedral layered lattice was found, and Rietveld refinement of its crystal structure was performed. The conductivity of the Na$_{0.8}$Fe$_{0.8}$Sn$_{0.2}$O$_2$ was of the sodium-cation type and at a room temperature of 10^{-8} S $\times$ cm^{-1} with the activation energy of 64.2 $\pm$ 0.43 kJ·mol^{-1}. A migration map was built using the Voronoi–Dirichlet approach. The radius of the elementary migration channel in the Na$_{0.8}$Fe$_{0.8}$Sn$_{0.2}$O$_2$ lattice was slightly smaller than the size critical for Na$^+$ cations in oxide compounds, which may be the reason why the sodium-cation conductivity of the Na$_{0.8}$Fe$_{0.8}$Sn$_{0.2}$O$_2$was rather low at low temperatures. The obtained results show that the application of the compound studied in this work as a solid electrolyte in sodium power sources is unlikely. It is the potential use of Na$_{0.8}$Fe$_{0.8}$Sn$_{0.2}$O$_2$ as the active material of cathodes in Na and Na-ion power sources that presents practical interest.

References

1. Julien, C. Technological Applications of Solid State Ionics. *Mater. Sci. Eng.* **1990**, *6*, 9–28. [CrossRef]
2. Jung, K.; Heo, H.-J.; Lee, J.-H.; Park, Y.C.; Kang, C.-Y. Enhanced corrosion resistance of Hypo-eutectic Al-1Mg-xSi alloys against molten sodium attack in high temperature sodium-sulfur batteries. *Corros. Sci.* **2015**, *98*, 748–757. [CrossRef]
3. Chang, R.; Minck, R. Sodium-sulfur battery flight experiment definition study. *J. Power Sources* **1990**, *29*, 555–563. [CrossRef]
4. Anantharamulu, N.; Koteswara Rao, K.; Rambabu, G.B.; Kumar, V.; Velchuri, R.; Vithal, M. A wide-ranging review on Nasicon type materials. *J. Mater. Sci.* **2011**, *46*, 2821–2837. [CrossRef]
5. Maruyama, T.; Saito, Y.; Matsumoto, Y.; Yano, Y. Potentiometric sensor for sulfur oxides using NASICON as a solid electrolyte. *Solid State Ion.* **1985**, *17*, 281–286. [CrossRef]
6. Bruce, P.G. Energy storage beyond the horizon: Rechargeable lithium batteries. *Solid State Ion.* **2008**, *179*, 752–760. [CrossRef]
7. Scrosati, B.; Garche, J. Lithium batteries: Status, properties and future. *J. Power Sources* **2010**, *195*, 2419–2430. [CrossRef]
8. Robertson, A.D.; West, A.R.; Ritchie, A.G. Review of crystalline lithium-ion conductors suitable for high temperature battery applications. *Solid State Ion.* **1997**, *104*, 1–11. [CrossRef]
9. Thangadurai, V.; Weppner, W. Recent progress in solid oxide and lithium ion conducting electrolytes research. *Ionics* **2006**, *12*, 81–92. [CrossRef]
10. Knauth, P. Inorganic solid Li-ion conductors: An overview. *Solid State Ion.* **2009**, *180*, 911–916. [CrossRef]
11. Bachman, J.C.; Muy, S.; Grimaud, A.; Chang, H.-H.; Pour, N.; Lux, F.S.; Paschos, O.; Maglia, S.; Lupart, S.; Lamp, P.; et al. Inorganic Solid-State Electrolytes for Lithium Batteries: Mechanisms and Properties Governing Ion Conduction. *Chem. Rev.* **2016**, *116*, 140–162. [CrossRef] [PubMed]
12. Hwang, J.-Y.; Myung, S.-T.; Sun, J.-K. Sun Sodium-ion batteries: Present and future. *Chem. Soc. Rew.* **2017**, *46*, 3529–3614. [CrossRef] [PubMed]
13. Nayak, P.K.; Yang, L.; Brehm, W.; Adelhelm, P. From Lithium-Ion to Sodium-Ion Batteries: Advantages, Challenges and Surprises. *Angew. Chem. Int. Ed.* **2018**, *57*, 102–120. [CrossRef]
14. Delmas, C. Sodium and Sodium-Ion Batteries: 50 Years of Research. *Adv. Energy. Mater.* **2018**, *8*, 1703137. [CrossRef]
15. Fergus, J.W. Ion transport in sodium ion conducting solid electrolytes. *Solid State Ion.* **2012**, *227*, 102–112. [CrossRef]

16. Meutzner, F.; Munchgesang, W.; Kabanova, N.A.; Zschornak, M.; Leisegang, T.; Blatov, V.A.; Meyer, D.C. On the Way to New Possible Na-Ion Conductors: The Voronoi-Dirichlet Approach, Data Mining and SymmetryConsideration in Ternary Na Oxides. *Chem. Eur. J.* **2015**, *21*, 16601–16608. [CrossRef]

17. Yang, C.; Xin, S.; Mai, L.; You, Y. Materials Design for High-Safety Sodium-Ion Battery. *Adv. Energy Mater.* **2020**, *11*, 2000974. [CrossRef]

18. Chayambuka, K.; Mulder, G.; Danilov, D.L.; Notten, P.H.L. Sodium-Ion Battery Materials and Electrochemical Properties Reviewed. *Adv. Energy. Mater.* **2018**, *8*, 1800079. [CrossRef]

19. Zhao, C.; Wang, Q.; Yao, Z.; Wang, J.; Sanchez-Lengeling, B.; Ding, F.; Qi, X.; Lu, Y.; Bai, X.; Li, B.; et al. Rational design of layered oxide materials for sodium-ion batteries. *Sciense* **2020**, *370*, 708–711. [CrossRef]

20. Skundin, A.M.; Kulova, T.L.; Yaroslavtsev, A.B. Sodium-Ion Batteries (A Review). *Russ. J.Electrochem.* **2018**, *54*, 131–174. [CrossRef]

21. Fedotov, S.S.; Kabanova, N.A.; Kabanov, A.A.; Blatov, V.A.; Khasanova, N.R.; Antipov, E.V. Crystallochemical tools in the search for cathode materials of rechargeable Na-ion batteries and analysis of their transport properties. *Solid State Ion.* **2018**, *314*, 129–140. [CrossRef]

22. Han, J.; Niu, Y.; Zhang, Y.; Jiang, J.; Bao, S.; Hu, M. Evaluation of O_3-type $Na_{0.8}Ni_{0.6}Sb_{0.4}O_2$ as cathode materials for sodium-ion batteries. *J. Solid State Electrochem.* **2016**, *20*, 2331–2335. [CrossRef]

23. Smirnova, O.A.; Fuentes, R.O.; Figueiredo, F.; Kharton, V.V.; Marques, F.M.B. Stability and Termal Expansion of Na^+-Conducting Ceramics. *J. Electroceram.* **2003**, *11*, 179–189. [CrossRef]

24. Li, X.; Wu, D.; Zhou, Y.N.; Liu, L.; Yang, X.-Q.; Ceder, G. A quaternary layered cathode compound or rechargeable Na ion batteries. *Electrochem. Commun.* **2014**, *49*, 51–54. [CrossRef]

25. Maazaz, A.; Delmas, C.; Fouassier, C.; Reau, J.-M.; Hagenmuller, P. Sur une nouvelle famille de formule $K_x(L_{x/2}Sn_{1-x/2})O_2$ (L = Mg, Ca, Zn; x < 1). *Mater. Res. Bull.* **1979**, *14*, 193–199. [CrossRef]

26. Delmas, C.; Fouassier, C.; Hagenmuller, P. Structural classification and properties of the layered oxides. *Phys. BC* **1980**, *99*, 81–85. [CrossRef]

27. Yoshida, H.; Yabuuchi, N.; Komaba, S. $NaFe_{0.5}Co_{0.5}O_2$ as high energy and power positive electrode for Na-ionbatteries. *Electrochem. Commun.* **2013**, *80*, 716–719. [CrossRef]

28. Zhao, J.; Zhao, L.; Dimov, N.; Okada, S.; Nashida, T. Electrochemical and Thermal Properties of α-$NaFeO_2$ Cathodefor Na-Ion Batteries. *J. Electrochem. Soc.* **2013**, *160*, A3077–A3081. [CrossRef]

29. Thorne, J.S.; Chowdhury, S.; Dunlap, R.A.; Obrovac, M.N. Structure and Electrochemistry of$Na_xFe_xTi_{1-x}O_2$ (1.0 ≥ x ≥ 0.75) for Na-Ion Battery Positive Electrodes. *J. Electrochem. Soc.* **2014**, *161*, A1801–A1805. [CrossRef]

30. Susanto, D.; Cho, M.K.; Ghulam, A.; Kim, J.-Y.; Chang, H.J.; Kim, H.-S.; Nam, K.-W.; Chung, K.Y. Anionac Redox Acivity as a Key Factor in the Performance Degradation of $NaFeO_2$ Cathodes for Sodium Ion Batteries. *Chem. Mater.* **2019**, *31*, 3644–3651. [CrossRef]

31. Li, C.; Reid, A.F.; Saunders, S. Nonstoihiometric Alkali Ferrites and Aluminates in the Systems $NaFeO_2$-TiO_2,$KFeO_2$-TiO_2, $KAlO_2$-TiO_2 and $KAlO_2$-SiO_2. *J. Solid State Chem.* **1971**, *3*, 614–620. [CrossRef]

32. Burmakin, E.I.; Shekhtman, G.S. Solid electrolytes in the Fe_2O_3-TiO_2-Na_2O system. *Elektrokhimiya* **1985**, *21*, 752–757. (In Russian)

33. Rodriguez-Carvajal, J. Recent advances in magnetic structure determination by neutron powder diffraction. *Physica* **1993**, *192B*, 55–69. [CrossRef]

34. Anurova, N.A.; Blatov, V.A. Analysis of ion-migration paths in inorganic frameworks by means of tilings and Voronoi–Dirichlet partition: A comparison. *Acta Cryst.* **2009**, *65*, 426–434. [CrossRef]

35. Anurova, N.A.; Blatov, V.A.; Ilyushin, G.D.; Blatova, O.A.; Ivanov-Schits, A.K.; Demy'anets, L.N. Migration maps of Li^+ cations in oxygen-containing compounds. *Solid State Ion.* **2008**, *179*, 2248–2254. [CrossRef]

36. Takeda, Y.; Akagi, J.; Edagawa, A.; Inagaki, M.; Naka, S. A preparation and polymorphic relations of sodium iron oxide ($NaFeO_2$). *Mat. Res. Bull.* **1980**, *15*, 1167–1172. [CrossRef]

37. Collongues, R.; Thery, J. Preparation et Proprietes des Ferrites de Sodium. *Bull. Soc. Chim. France* **1959**, *51*, 1141–1144. [CrossRef]

38. West, A.R. $NaAlO_2$ and $NaFeO_2$Polymorphism. *Nature* **1974**, *249*, 245–246. [CrossRef]

39. Grey, I.E.; Hill, R.J.; Hewatt, A.W. A neutron powder diffraction study of the β to γ phase transformation in $NaFeO_2$. *Z. Krist.* **1990**, *193*, 51–69. [CrossRef]

40. Ito, J.; Frondel, C. Synthetic zirconium and titanum garnets. *Amer. Mineral.* **1967**, *52*, 773–781.

41. Shannon, R.D. Revised effective ionic radii and systematic studies of interatomic distances in halides and chalcogenides. *Acta Cryst.* **1976**, *32*, 751–767. [CrossRef]

42. Breger, J.; Jiang, M.; Dupre, N.; Meng, Y.S.; Yang, S.-H.; Ceder, G.; Grey, C.P. High-resolution X-ray diffraction, DIFFaX, NMR and first principles study of disorder in the Li_2MnO_3—$Li[Ni_{1/2}Mn_{1/2}]O_2$ solid solutions. *J. Solid State Chem.* **2005**, *178*, 2575–2585. [CrossRef]

43. Baroudi, K.; Yim, C.; Wu, H.; Huang, O.; Roudebush, J.H.; Vavilova, E.; Grafe, H.-J.; Kataev, V.; Buechner, B.; Ji, H.; et al. Structure and properties of α-$NaFeO_2$-type ternary sodium iridates. *J. Solid State Chem.* **2014**, *210*, 195–205. [CrossRef]

44. Blatov, V.A. Multipurpose crystallochemical analysis with the program package TOPOS. *IUCr Comput. Comm. Newsl.* **2006**, *7*, 4.

45. Fedotov, S.S.; Kabanov, A.A.; Kabanova, N.A.; Blatov, V.A.; Zhugayevych, A.; Abakumov, A.M.; Khasanova, N.R.; Antipov, E.V. Crystal Structure and Li-Ion Transport in Li$_2$CoPO$_4$F High-Voltage Cathode Material for Li-Ion Batteries. *J. Phys. Chem.* **2017**, *121C*, 3194–3202. [CrossRef]

46. Sridharan, R.; Gnanasekaran, T.; Mathews, C.K. Phase equilibrium studies in the Na-Fe-O system. *J. Alloys Compd.* **1993**, *191*, 9–13. [CrossRef]